Redox Biology 75 (2024) 103277

Contents lists available at ScienceDirect

Redox Biology

journal homepage: www.elsevier.com/locate/redox

TrxR1 is involved in the activation of Caspase-11 by regulating the oxidative-reductive status of Trx-1

Dongsheng Bai [a,1], Chen Zhou [a,1], Jiaying Du [a], Jiawei Zhao [a], Chunyang Gu [a], YuXiang Wang [a], Lulu Zhang [b,**], Na Lu [a,***], Yue Zhao [a,*]

[a] State Key Laboratory of Natural Medicines, Jiangsu Key Laboratory of Carcinogenesis and Intervention, Department of Physiology, School of Basic Medicine and Clinical Pharmacy, China Pharmaceutical University, 24 Tongjiaxiang, Nanjing, 210009, China
[b] Department of Clinical Pharmacology, School of Pharmacy, Nanjing Medical University, Nanjing, China

ARTICLE INFO

Keywords:
TrxR
Thioredoxin-1
Caveolin-1
Outer membrane vesicle
Caspase-11

ABSTRACT

Sepsis is a common complication of infections that significantly impacts the survival of critically patients. Currently, effective pharmacological treatment strategies are lacking. Auranofin, known as an inhibitor of Thioredoxin reductase (TrxR), exhibits anti-inflammatory activity, but its role in sepsis is not well understood. Here, we demonstrate the significant inhibitory effect of Auranofin on sepsis in a cecal ligation and puncture (CLP) mouse model. *In vitro*, Auranofin inhibits pyroptosis triggered by Caspase-11 activation. Further investigations reveal that inhibiting TrxR1 suppresses macrophage pyroptosis induced by *E. coli*, while TrxR2 does not exhibit this effect. TrxR1, functioning as a reductase, regulates the oxidative-reductive status of Thioredoxin-1 (Trx-1). Mechanistically, the modulation of Trx-1's reductive activity by TrxR1 may be involved in Caspase-11 activation-induced pyroptosis. Additionally, inhibiting TrxR1 maintains Trx-1 in its oxidized state. The oxidized form of Trx-1 interacts with Caveolin-1 (CAV1), regulating outer membrane vesicle (OMV) internalization. In summary, our study suggests that inhibiting TrxR1 suppresses OMV internalization by maintaining the oxidized form of Trx-1, thereby restricting Caspase-11 activation and alleviating sepsis.

Abbreviations:

TrxR	Thioredoxin reductase
Caspase	Cysteinyl aspartate specific proteinase
Trx-1	Thioredoxin-1
CLP	Cecal ligation and puncture
CAV1	Caveolin-1
OMV	Outer membrane vesicle
LPS	Lipopolysaccharide
GSDMD	Gasdermin D
CME	Clathrin-mediated endocytosis
CavME	Caveolae-mediated endocytosis
GBP	Guanylate-binding protein
ROS	Reactive oxygen species
BMDM	Bone marrow-derived macrophage
LDH	Lactate dehydrogenase
LAL	Limulus amebocyte lysate
CTxB	Cholera toxin subunit B
LATA	Latrunculin A
WT	Wild-type
DTT	Dithiotriol
NLRP1	Nod-like receptor
DMSO	Dimethyl sulfoxide
HRP	Horseradish peroxidase

(*continued on next column*)

(*continued*)

1. Introduction

In the context of sepsis, a severe inflammatory response triggered by bacterial infection emerges as a prominent causative factor [1,2]. Lipopolysaccharide (LPS), a principal constituent of the outer membrane of Gram-negative bacteria, possesses the potential to induce a dysregulated immune response during sepsis [3]. The inflicted tissue damage, a

* Corresponding author.
** Corresponding author.
*** Corresponding author.
E-mail addresses: lulu_0219@njmu.edu.cn (L. Zhang), nalu@cpu.edu.cn (N. Lu), yuezhao@cpu.edu.cn (Y. Zhao).
[1] These authors contributed equally to this work.

https://doi.org/10.1016/j.redox.2024.103277
Received 29 May 2024; Received in revised form 15 July 2024; Accepted 20 July 2024
Available online 20 July 2024

consequence of macrophage excessive activation by LPS, intricately hinges on the initiation of Caspase-11 [4]. By recognizing LPS in the cytoplasm, Caspase-11 processes gasdermin D (GSDMD) into a pore-forming peptide, thereby culminating in pyroptosis [5,6]. Substantiating this notion is an expanding body of evidence indicating that Caspase-11-mediated pyroptosis plays a pivotal role in sepsis-related mortality, disrupting local immune homeostasis by exacerbating vascular permeability [7,8]. Nonetheless, it is crucial to note that only LPS delivered into the cytoplasm has the capacity to activate Caspase-11 [8,9]. Given that LPS is a critical constituent of the outer membrane of Gram-negative bacteria, it can bind not only to pattern recognition receptors on the cell surface but also be transported into the cytoplasm through outer membrane vesicles (OMVs) [10]. Consequently, impeding the delivery of LPS via OMVs emerges as a promising therapeutic approach for the management of sepsis [11].

The uptake of OMVs into the cytoplasm has been ascertained to occur via endocytosis [12,13]. The endocytosis pathway encompasses clathrin-mediated endocytosis (CME) and caveolae-mediated endocytosis (CavME) [14]. In CME, clathrin assembles around membrane pits, generating a polygonal lattice structure which, in turn, facilitates the formation of large vesicles, thus promoting the entry of OMVs into the cytoplasm [15]. Additionally, OMVs can gain access to the cytoplasm via membrane invagination mediated by caveolin [16]. Upon internalization, OMVs subsequently engage in membrane fusion events with endosomes, culminating in the release of LPS into the cytoplasm [17]. Subsequently, LPS augments Caspase-11 activation and pyroptosis through its interaction with guanylate-binding proteins (GBPs) [18]. Hence, OMV endocytosis constitutes a pivotal step in the delivery of LPS, yet the regulatory mechanisms governing this process remain elusive [10].

Oxidative stress refers to the generation of reactive oxygen species (ROS) and the disruption of the protective mechanisms, often concomitant with the onset of inflammation [19]. Endocytosis frequently correlates with alterations in oxidative stress levels, yet the regulatory association between these processes remains unclear [20]. In coping with cellular oxidative stress, the thioredoxin system plays an important role. Thioredoxin reductase (TrxR) specifically catalyzes the NADPH-dependent reduction of thioredoxin (Trx) to maintain its reduced state. Thioredoxin is a ubiquitous enzyme that catalyzes thiol-disulfide exchange reactions, relying on a conserved active site containing two cysteine residues, which can be oxidized to form a reversible disulfide bond. Thioredoxin not only maintains redox homeostasis, but also participates in the regulation of cell death. On the one hand, it is suggested that Trx-1 triggers apoptosis under oxidative stress by regulating the release of ASK1 or directly regulating the S-nitrosation of Caspase-3 [21–23]. On the other hand, Trx-1 affects pyroptosis by regulating the NLRP3 or NLRP1 inflammasome [24,25]. Although these studies have revealed the regulation of oxidative stress on cell homeostasis, the mechanism of Caspase-11 activation of pyroptosis remains unclear. In this study, we present evidence that the inhibition of TrxR1 mitigates sepsis and suppresses Caspase-11 activation. Notably, our findings reveal that TrxR1 inhibition maintains Trx-1 in an oxidized state (disulfide), rather than a reduced state (dithiol). The oxidized form of Trx-1 can interact with caveolin 1 (CAV1), modulating OMV endocytosis. Collectively, these results illuminate that cellular reductive stress may serve as an inflammatory signal for Caspase-11 activation.

2. Results

2.1. Auranofin alleviates sepsis induced by cecal puncture and ligation in vivo

The Auranofin, a TrxR inhibitor, was selected for the treatment of sepsis. The results showed that Auranofin significantly reduced the mortality of sepsis caused by CLP in mice (Fig. 1A). Histopathological analysis of liver and lung in mice revealed that Auranofin effectively alleviated CLP-induced tissue damage, hemorrhaging, and infiltration of inflammatory cells (Fig. 1B). Furthermore, Auranofin exhibited a noteworthy reduction in the increase of spleen weight induced by sepsis (Fig. 1C). The results also indicated that Auranofin attenuated the elevations in sepsis-induced levels of LDH, BUN, and ALT (Fig. 1D). When applied in the context of intestinal bacterial infections resulting from appendix puncture, Auranofin significantly diminished bacteria burden in the blood of mice (Fig. 1E). Moreover, in septic mice, serum concentrations of proinflammatory cytokines such as TNF-α, IL-1β, and IL-18 exhibited marked increases, which were effectively mitigated by Auranofin (Fig. 1F). Notably, the expression of Cleaved-Caspase-11 and GSDMD-N in liver and lung tissues displayed significant reductions following Auranofin treatment (Fig. 1G and H). Collectively, these *in vivo* studies provide compelling evidence that Auranofin ameliorated tissue damage caused by sepsis.

2.2. Auranofin inhibits Caspase-11 activation and pyroptosis induced by E. coli infection in vitro

The occurrence of sepsis is intricately linked to the overactivation of macrophages. To explore the impact of Auranofin on macrophage activation, pyroptosis was induced by *E. coli* infection. This infection led to a significant reduction in cell viability in both J774A.1 cells and mouse bone marrow-derived macrophages (BMDMs). Remarkably, Auranofin counteracted the decline in cell viability triggered by *E. coli* infection (Fig. 2A). The occurrence of pyroptosis was associated by the release of lactate dehydrogenase (LDH). Notably, Auranofin attenuated the LDH release induced by *E. coli* infection (Fig. 2B). During the course of *E. coli* infection, the structural integrity of the cell membrane was compromised, allowing PI-tagged nucleic acid to penetrate the cells. The results of the PI uptake assay demonstrated that Auranofin mitigated the disruption of the cell membrane structure (Fig. 2C). Pyroptosis coincided with the release of IL-1β, which was significantly inhibited by Auranofin in response to *E. coli* infection (Fig. S1A). Additionally, pyroptosis caused by *E. coli* infection necessitated the activation of Caspase-11 inflammasome. Western blot analysis revealed that Auranofin significantly suppressed the activation of Caspase-11 (p26) and formation of GSDMD-N induced by *E. coli* infection (Fig. 2D). Meanwhile, the enzymatic activity of TrxR is also significantly inhibited by Auranofin (Fig. 2E). Activation of Caspase-11 by E. *coli* is contingent upon the levels of LPS in the cytoplasm. To assess the cytoplasmic LPS levels, digitonin extraction from macrophage cytoplasm and limulus amebocyte lysate (LAL) assay were employed. Notably, the plasma membrane, early and late endosomes, and lysosomes (Na^+/K^+ ATPase, EEA1, Rab7, and LAMP1) were absent from the cytosol extracted with digitonin (Fig. S1B). However, Auranofin significantly reduced LPS levels in the cytoplasm (Fig. 2F). In contrast, no significant changes were observed in bacteria within residual fractions (Fig. 2G). This indicates that Auranofin did not affect the adherence of *E. coli*. Collectively, these results suggest that Auranofin inhibits *E. coli* infection-induced pyroptosis.

2.3. TrxR1, but not TrxR2, regulates E. coli infection-induced pyroptosis

While Auranofin is commonly regarded as a TrxR inhibitor, its selectivity is limited. We established J774A.1 cell lines with either Txnrd1 or Txnrd2 knockdown to investigate their specific roles. Our findings indicated that Txnrd1 knockdown effectively mitigated the reduction in cell viability induced by *E. coli* (Figs. S2A and S2B). Additionally, the reduction in LDH release was concomitant with the knockdown of Txnrd1 (Fig. S2C). Furthermore, we observed a significant reduction in PI uptake following Txnrd1 knockdown (Fig. S2D). Moreover, the knockdown of Txnrd1 resulted in the inhibition of IL-1β secretion, Caspase-11 (p26) activation and GSDMD-N formation (Figs. S2E and S2F). Intriguingly, the knockdown of Txnrd1 reduced LPS

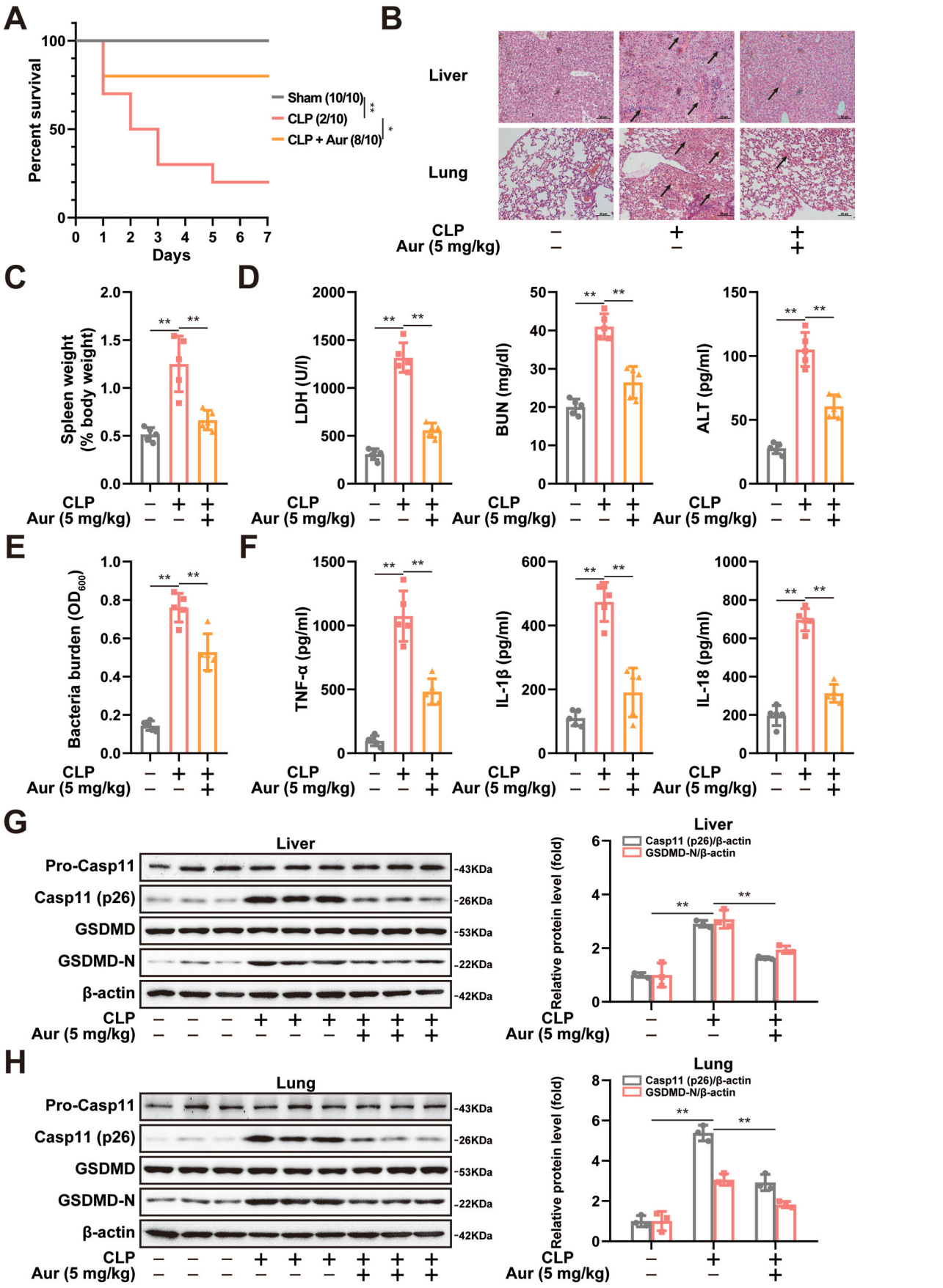

(caption on next page)

Fig. 1. Auranofin alleviates CLP-induced sepsis in mice. (A) Analysis of animal survival in mice with or without intraperitoneal administration of Auranofin (5 mg/kg) after CLP-induced sepsis (Kaplan-Meier survival analysis). n = 10 per group. (B) Representative images of H&E stains of liver and lung in mice from indicated group. Scale bars: 50 μm. (C) The ratio of spleen weight to percentage of body weight in mice from indicated group. n = 5 per group. (D) The LDH, BUN and ALT levels in the serum of the indicated group mice. n = 5 per group. (E) Bacteria burden in the blood of the indicated group mice. n = 5 per group. (F) Analysis of serum levels of TNF-α, IL-1β and IL-18 in the indicated group mice. n = 5 per group. (G and H) Western blot analysis of Caspase-11 (Casp11) and GSDMD expression in the liver tissues(G) or lung tissues(H) of the indicated group mice. β-actin served as the loading control. n = 3 per group. The values are expressed as the mean ± SD, $*p < 0.05$, $**p < 0.01$.

levels in the cytoplasm (Fig. S2G). In contrast, Txnrd2 knockdown had no discernible impact on cell viability or LDH release (Figs. S3A–S3C). These comprehensive findings collectively suggest that TrxR1, in contrast to TrxR2, plays a pivotal role in regulating pyroptosis in response to *E. coli* infection.

2.4. The regulation of pyroptosis by TrxR1 depends on Trx-1

To elucidate the precise mechanism governing the regulation of pyroptosis by TrxR1, we constructed a mutant variant of Txnrd1 (C59S), which carries a mutation at its active enzymatic site (Fig. S4A). Our findings revealed that rescue of wild-type Txnrd1 significantly reduced cell viability in J774A.1 cells with Txnrd1 knockdown. Conversely, the rescue of the active site mutation in Txnrd1 exhibited no discernible impact on cell viability (Fig. 3A). Consistently, the restoration of wild-type Txnrd1 resulted in a marked increase in LDH release and IL-1β secretion, whereas the restoration of mutant Txnrd1 had no effect on LDH release and IL-1β secretion (Fig. 3B and S4B). Notably, we observed no significant alterations in the amount of bacteria were detected in the residual component between experimental groups (Fig. S4C). However, the restoration of wild-type Txnrd1 was associated with elevated cytoplasmic LPS levels, whereas the restoration of mutant Txnrd1 had no impact on cytoplasmic LPS levels (Fig. 3C). Western blot analyses further corroborated our findings, demonstrating that depletion of Txnrd1 led to a significant decrease in Caspase-11 (p26) activation, and GSDMD-N formation. Conversely, the rescue of wild-type Txnrd1 induced a substantial increase in the levels of these proteins. Intriguingly, Txnrd1 with the active site mutation failed to exert any influence on the expression of these proteins (Fig. 3D). Collectively, these results provide evidence supporting that the regulatory role of TrxR1 in pyroptosis is contingent upon its enzymatic activity.

It is well-established that TrxR1 functions as a reductase, regulating the redox state of Trx-1. Therefore, in order to gain further insights, we knocked down both Txnrd1 and Txn (Fig. S4D). Our results reveal that the recovery of cell viability induced by Txnrd1 knockdown was abolished after Txnrd1 and Txn concurrent knockdown (Fig. 3E). The LDH release and IL-1β secretion also underwent similar changes in Txnrd1 and Txn knockdown J774A.1 cells (Fig. 3F and S4E). Remarkably, no significant alterations in the amount of bacteria were detected in the residual components (Fig. S4F). However, cytoplasmic LPS levels exhibited a significant increase in response to knockdown of Txnrd1 and Txn (Fig. 3G). These results further suggest that the regulation of pyroptosis by TrxR1 depends on Trx-1.

2.5. TrxR1 governs pyroptosis by maintaining the reductive activity of Trx-1

To validate the involvement of Trx-1 reductive activity in the regulatory of TrxR1 on pyroptosis, we constructed the active site mutant Txn (C32/35S). Our findings underscore that the restorative impact on pyroptosis inhibition conferred by Txnrd1 knockdown was only upon wild-type Trx-1, not upon mutant Trx-1 (Fig. 4A-C). Correspondingly, the inhibition of Caspase-11 (p26) activation and GSDMD-N formation induced by Txnrd1 knockdown could be restored by expressing wild-type Trx-1. However, expressing the active site mutation of Trx-1 did not have these effects (Fig. 4D). In addition, similar changes were produceds in cytoplasmic LPS levels (Fig. 4E). Furthermore, this relationship between TrxR1 and pyroptosis regulation, specifically through maintaining Trx-1 reductive activity, was substantiated using additional TrxR1 inhibitors (gamboic acid and DNCB) and hydrogen peroxide. Results demonstrated that both gamboic acid (GA) and DNCB, but not H_2O_2, inhibited LDH release induced by *E. coli* infection (Fig. 4F). Strikingly, the inhibitory effects of GA and DNCB on LDH release were nullified upon Txn knockdown (Fig. 4G). These data highlight the pivotal role of TRX1 reductive activity regulation in impeding *E. coli*-induced pyroptosis, without perturbing cellular redox balance.

2.6. TrxR1 regulates cytosolic LPS levels by participating in the uptake of OMVs

Endocytosis of OMVs carrying *E. coli*-released LPS occurs, leading to their cytoplasmic release via early endosomes. Consequently, an investigation into LPS colocalization with the early endosome marker Rab5 indicated that Txnrd1 knockdown resulted in reduced LPS colocalization with Rab5 (Fig. 5A). Fusion sorting of early endosomes yields late endosomes, subsequently merging with lysosomes for degradation. Notably, the knockdown of Txnrd1 also reduces the colocalization of LPS with the late endosome marker Rab7 (Fig. 5B). This prompts speculation that TrxR1 inhibition might enhance lysosomal degradation of LPS. To validate this hypothesis, we treated with the lysosomal inhibitor CQ. However, CQ failed to reverse the diminished LPS and Rab5 colocalization induced by Txnrd1 knockdown, nor did it reverse the decrease of LPS in the cytoplasm (Fig. 5C and D). These results suggest that TrxR1 does not regulate intracellular LPS via endosome-lysosomal degradation. Subsequently, the OMV endocytosis was significant reduced upon Txnrd1 knockdown (Fig. 5E). Utilizing the cholera toxin subunit B (CTxB) uptake assay, we observed impaired transport of CTxB to the perinuclear region following Txnrd1 knockdown. Interestingly, concurrent knockdown of both Txnrd1 and Txn restored CTxB endocytosis. Expression of wild-type Trx-1 reversed the inhibition of CTxB endocytosis by Txnrd1 knockdown, whereas expressing active site mutant Trx-1 did not (Fig. 5F). As CTxB is a confirmed marker of caveolae-mediated endocytosis, these findings suggest that TrxR1 may regulates caveolae-mediated endocytosis processes. Contrary to previous studies indicating OMV uptake via clathrin-mediated endocytosis, treatment with caveolin-endocytosis inhibitors, Filipin and Latrunculin A (LATA), blocked IL-1β secretion, Caspase-11 (p26) activation, and GSDMD-N formation (Figs. S5A and S5B). This implies that TrxR1 may modulate caveolae-mediated endocytosis to regulate OMV uptake.

2.7. Oxidized Trx-1 exhibits an affinity for caveolin-1

In the context of caveolae-mediated endocytic pathways, caveolin-1 (CAV1) plays a pivotal role in vesicle formation and subsequent cargo internalization. Considering the potential regulatory role of TrxR1 in caveolae-mediated endocytosis and OMV uptake, we investigated the colocalization of Trx-1 with CAV1. Immunofluorescence results revealed that Txnrd1 knockdown enhances the colocalization of Trx-1 with CAV1, with only the wild-type Trx-1 showing colocalization with CAV1, while the catalytically inactive site-mutated Trx-1 does not exhibit this colocalization (Fig. 6A). Subsequently, the interaction between Trx-1 and CAV1 was identified (Fig. 6B). As a key protein in maintaining redox balance, the reductive capacity of Trx-1 depends on the interaction between Cys32 and disulfide bonds in oxidized proteins. Subsequently, Cys35 mediates the dissolution of disulfide bonds between the target protein and Trx-1. To determine whether Cys32 and Cys35 are

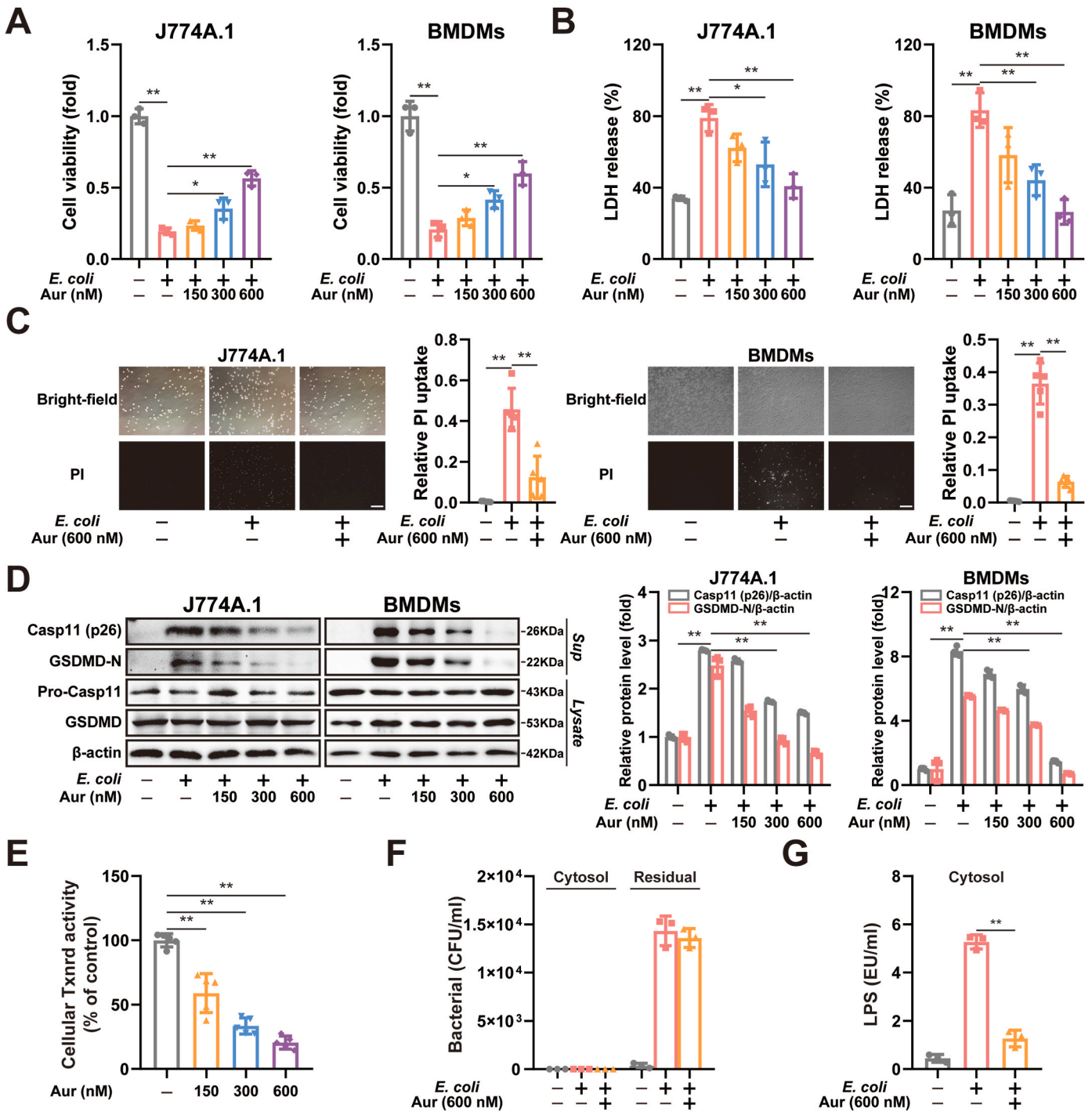

Fig. 2. Auranofin inhibits pyroptosis and Caspase-11 inflammasome activation in macrophages. (A) Analysis of cell viability in *E. coli*-infected J774A.1 or BMDMs treated with different concentrations Auranofin. n = 3 per group. (B) Analysis of LDH release in *E. coli*-infected J774A.1 or BMDMs treated with different concentrations Auranofin. n = 3 per group. (C) Analysis of PI uptakes in *E. coli*-infected J774A.1 or BMDMs treated with different concentrations Auranofin. n = 5 per group. (D) Western blot analysis of Caspase-11 and GSDMD expression in supernatants (Sup) and lysate in *E. coli*-infected J774A.1 or BMDMs, which treated with different concentrations Auranofin. n = 3 per group. (E) Analysis of TrxR1 activity in J774A.1 cells treated with different concentrations Auranofin. n = 5 per group. (F) Agar plating for bacterial counts in the cytosolic and residual fractions of *E. coli*-infected J774A.1 cells treated with different Auranofin. n = 3 per group. (G) LAL assay for LPS (EU, endotoxin units) in the cytosolic fractions of *E. coli*-infected J774A.1 cells treated with Auranofin. n = 3 per group. The values are expressed as the mean ± SD, $*p < 0.05$, $**p < 0.01$.

critical for CAV1 binding, we expressed WT, C32S, C35S, or C32S/C35S Trx-1. Notably, both Cys32 and Cys35 were found to be imperative for the binding (Fig. 6C). Additionally, the promotion of Trx-1 binding to CAV1 was observed upon the use of alternative TrxR1 inhibitors (Fig. 6D). These findings suggest the possibility that CAV1 selectively interacts with the oxidized form of Trx-1. Subsequently, anti-Flag magnetic beads will be treated with the oxidizing agent hydrogen peroxide (H_2O_2) or the reducing agent dithiotriol (DTT), immobilized by Flag-tagged CAV1 protein in future experiments. Interestingly, H_2O_2 was observed to enhance the Trx-1 interaction, whereas DTT abolished the interaction, affirming that only oxidized Trx-1 binds to CAV1 (Fig. 6E). Furthermore, auranofin facilitated the CAV1 binding of wild-

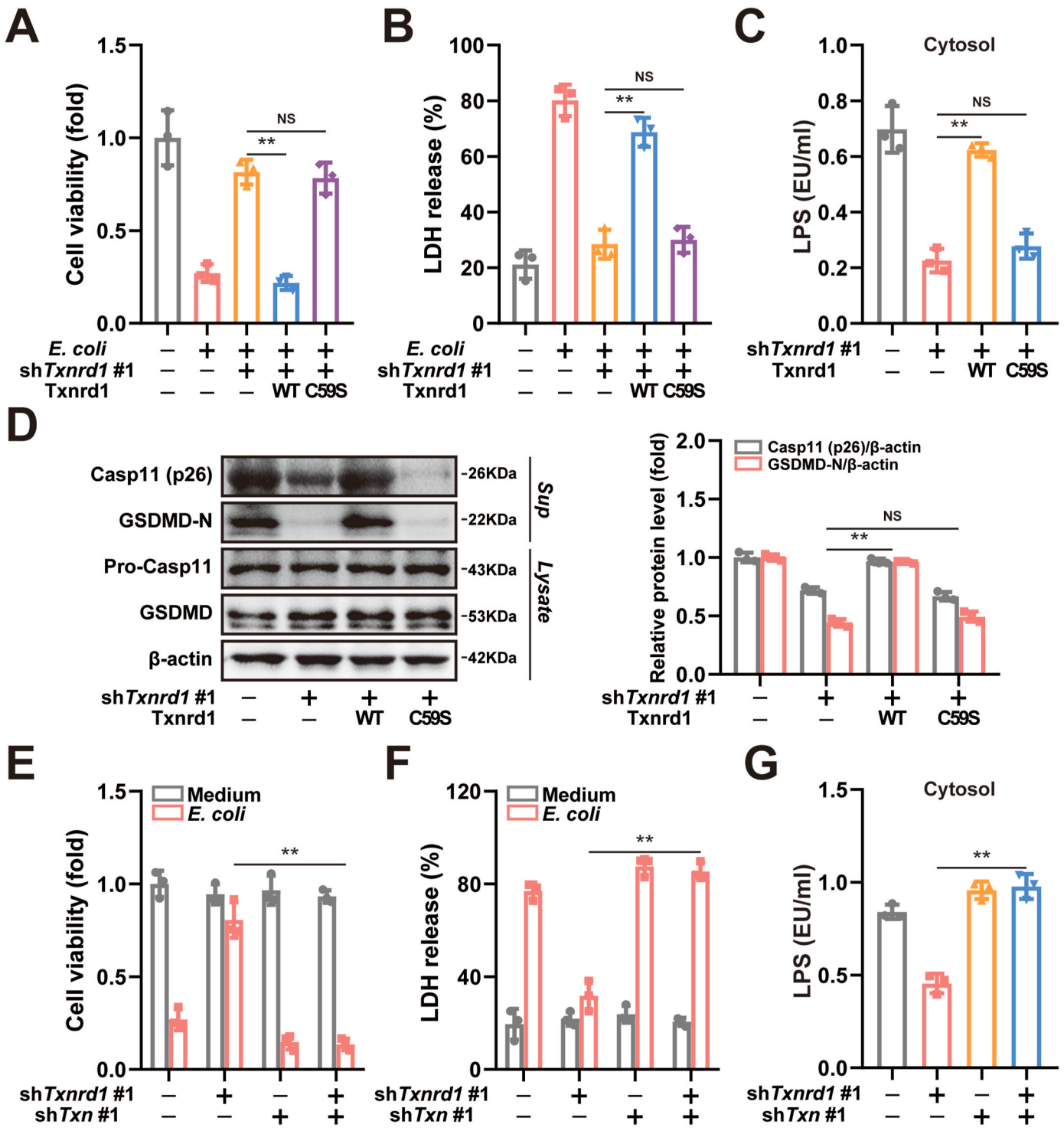

Fig. 3. Trx-1 involves in the regulation of TrxR1 on pyroptosis and Caspase-11 inflammasome activation in macrophages. (A) Analysis of cell viability in *E. coli*-infected J774A.1 cells expressing Txnrd1 shRNA and Txnrd1 WT or C59S variant cDNA. n = 3 per group. (B) Analysis of LDH release in *E. coli*-infected J774A.1 cells expressing Txnrd1 shRNA and Txnrd1 WT or C59S variant cDNA. n = 3 per group. (C) LAL assay for LPS (EU, endotoxin units) in the cytosolic fractions of *E. coli*-infected J774A.1 cells expressing Txnrd1 shRNA and Txnrd1 WT or C59S variant cDNA. n = 3 per group. (D) Western blot analysis of Caspase-11 and GSDMD expression in supernatants (Sup) and lysate in *E. coli*-infected J774A.1 cells expressing Txnrd1 shRNA and Txnrd1 WT or C59S variant cDNA. n = 3 per group. (E) Analysis of cell viability in *E. coli*-infected J774A.1 cells expressing Txnrd1 and Txn shRNA. n = 3 per group. (F) Analysis of LDH release in *E. coli*-infected J774A.1 cells expressing Txnrd1 and Txn shRNA. n = 3 per group. (G) LAL assay for LPS (EU, endotoxin units) in the cytosolic fractions of *E. coli*-infected J774A.1 cells expressing Txnrd1 and Txn shRNA. n = 3 per group. The values are expressed as the mean ± SD, $^{**}p < 0.01$.

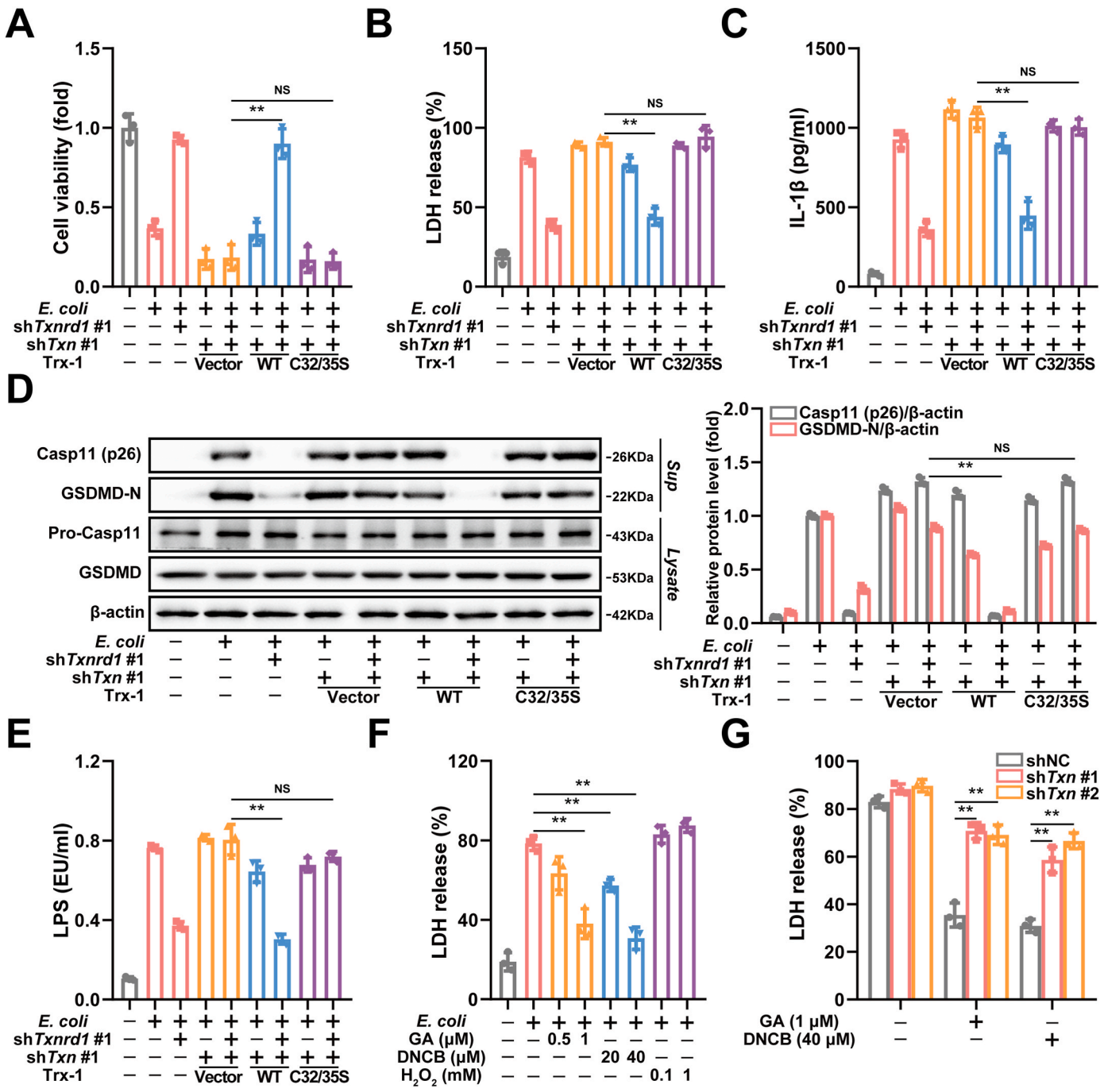

Fig. 4. TrxR1 controls pyroptosis and Caspase-11 inflammasome activation by maintaining the Trx-1 reductive activity. (A) Analysis of cell viability in *E. coli*-infected J774A.1 cells expressing Txnrd1 and Txn shRNA and Txn WT or C32/35S variant cDNA. n = 3 per group. (B) Analysis of LDH release in *E. coli*-infected J774A.1 cells expressing Txnrd1 and Txn shRNA and Txn WT or C32/35S variant cDNA. n = 3 per group. (C) Analysis of IL-1β in supernatants of *E. coli*-infected J774A.1 cells expressing Txnrd1 and Txn shRNA and Txn WT or C32/35S variant cDNA. n = 3 per group. (D) Western blot analysis of Caspase-11 and GSDMD expression in supernatants (Sup) and lysate in *E. coli*-infected J774A.1 cells expressing Txnrd1 and Txn shRNA and Txn WT or C32/35S variant cDNA. n = 3 per group. (E) LAL assay for LPS (EU, endotoxin units) in the cytosolic fractions of *E. coli*-infected J774A.1 cells expressing Txnrd1 and Txn shRNA and Txn WT or C32/35S variant cDNA. n = 3 per group. (F) Analysis of LDH release in *E. coli*-infected J774A.1 cells treated with GA, DNCB and H_2O_2. n = 3 per group. (G) Analysis of LDH release in *E. coli*-infected J774A.1 cells upon Txn knockdown treated with GA and DNCB. n = 3 per group. The values are expressed as the mean ± SD, $^*p < 0.05$, $^{**}p < 0.01$.

type Trx-1, while the C32S/C35S mutant Trx-1 failed to bind to CAV1 (Fig. 6F). To identify the specific domain of CAV1 involved in the interaction with Trx-1, we generated various truncated mutants of CAV1. Co-immunoprecipitation experiments revealed that the N-terminal domain of CAV1 interacts with Trx-1 (Fig. 6G).

2.8. TrxR1 sustains cellular membrane localization and protein levels of CAV1

Given the critical role of CAV1 in endocytic processes, we investigated the impact of Txnrd1 knockdown on cellular membrane localization of CAV1. Immunofluorescence experiments revealed

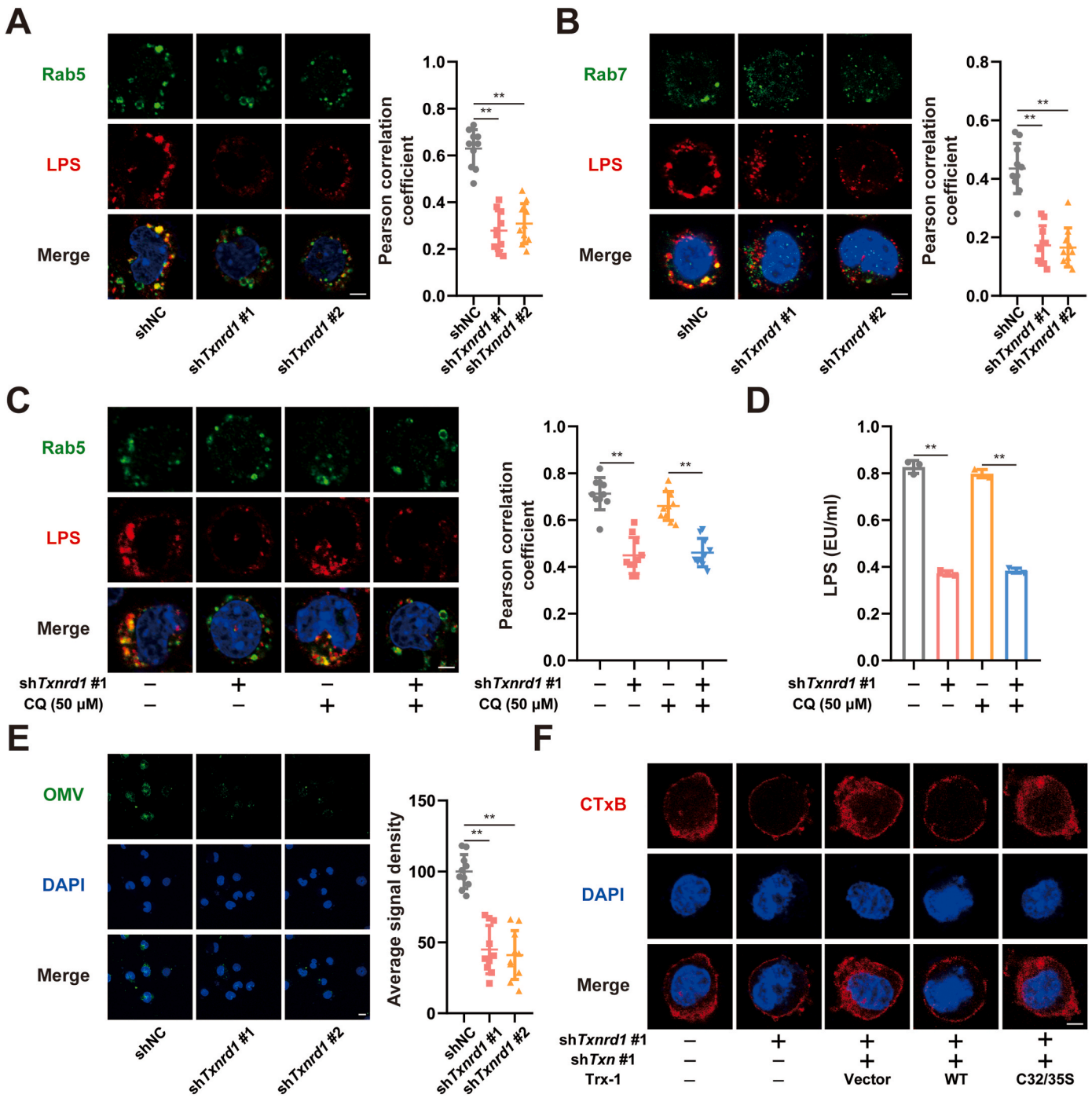

Fig. 5. TrxR1 controls the uptake of OMVs. (A) Intracellular distribution of Rab5 and LPS in *E. coli*-infected J774A.1 cells expressing Txnrd1 shRNA. Scale bars: 10 μm. Pearson's correlation coefficients for the co-localization of Rab5 with LPS from multiple confocal images. n = 10 per group. (B) Intracellular distribution of Rab7 and LPS in *E. coli*-infected J774A.1 cells expressing Txnrd1 shRNA. Scale bars: 10 μm. Pearson's correlation coefficients for the co-localization of Rab5 with LPS from multiple confocal images. n = 10 per group. (C) Intracellular distribution of Rab5 and LPS in *E. coli*-infected J774A.1 cells treated with Auranofin or CQ. Scale bars: 10 μm. Pearson's correlation coefficients for the co-localization of Rab5 with LPS from multiple confocal images. n = 10 per group. (D) LAL assay for LPS (EU, endotoxin units) in the cytosolic fractions of *E. coli*-infected J774A.1 cells treated with Auranofin or CQ. n = 3 per group. (E) The endocytosis of DiO-labeled OMVs in J774A.1 cells upon Txnrd1 knockdown. Scale bars: 10 μm. The average signal density of internalized green fluorescent OMVs. n = 10 per group. (F) The fluorescent of Alexa555-conjugated Cholera Toxin Subunit B (CTxB) in J774A.1 cells expressing Txnrd1 and Txn shRNA and Txn WT or C32/35S variant cDNA. Scale bars: 10 μm. The values are expressed as the mean ± SD, $^{**}p < 0.01$. (For interpretation of the references to colour in this figure legend, the reader is referred to the Web version of this article.)

colocalization of CAV1 with the cell membrane localization probe PM-mAG1. Upon Txnrd1 knockdown, a significant reduction in the cell membrane localization of CAV1 was observed. Simultaneous knockdown of Txnrd1 and Txn resulted in a notable restoration of CAV1 cell membrane localization. Subsequent reintroduction of Trx-1 showed that wild-type Trx-1 nearly abolished the cell membrane localization of CAV1, while reintroduction of mutated Trx-1 had no effect on CAV1 cell membrane localization (Fig. 7A). These results collectively indicate that TrxR1 maintains the cell membrane localization of CAV1. It has been reported that CAV1 unable to localize to the cell membrane undergoes

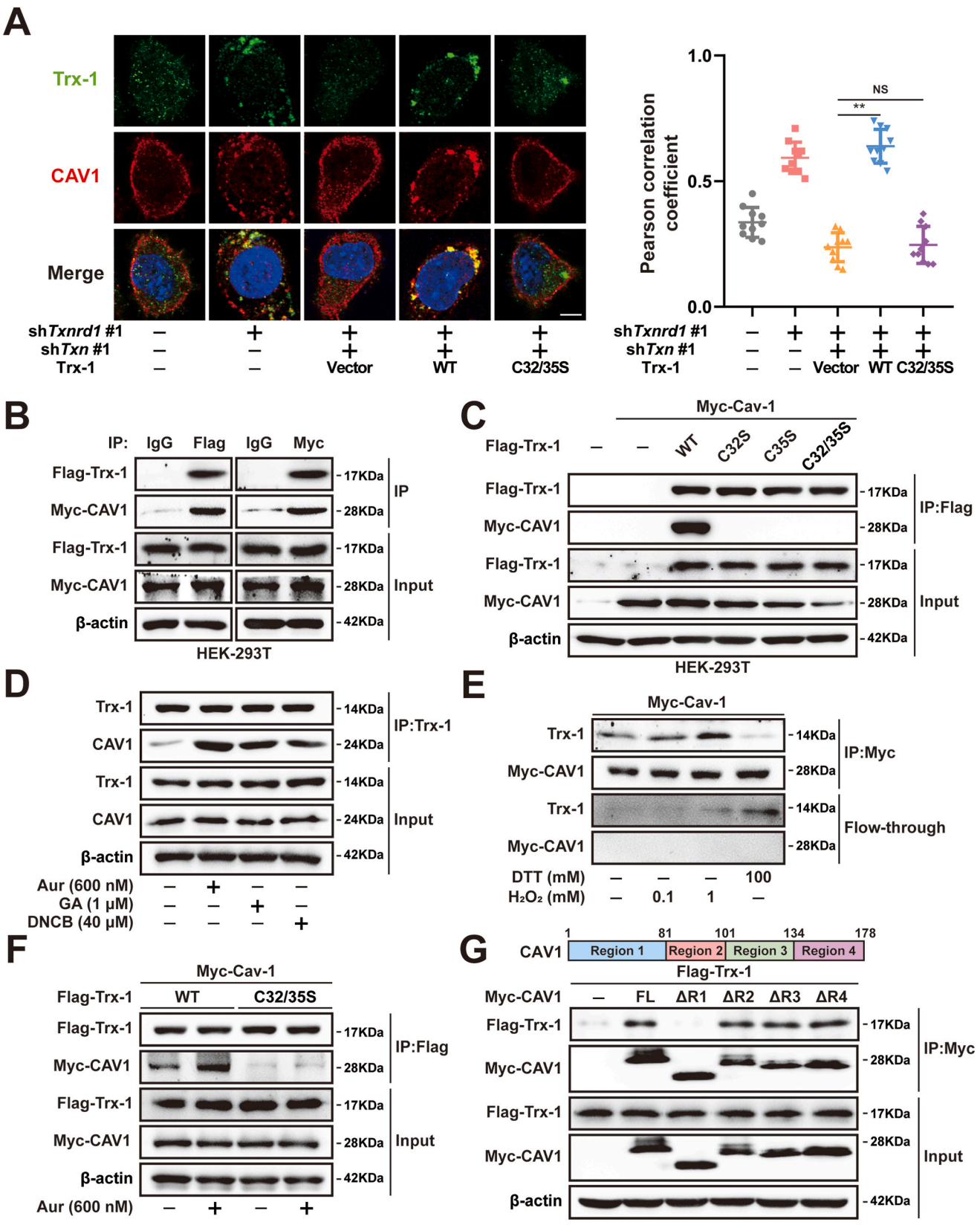

Fig. 6. Oxidized Trx-1 binds to CAV1. (A) Intracellular distribution of Trx-1 and CAV1 in *E. coli*-infected J774A.1 cells expressing Txnrd1 and Txn shRNA and Txn WT or C59S variant cDNA. Scale bars: 10 μm. Pearson's correlation coefficients for the co-localization of Trx-1 with CAV1 from multiple confocal images. n = 10 per group. (B) The interaction between Trx-1 and CAV1 in HEK-293T cells. (C) The binding of WT, C32S, C35S or C32/35S Trx-1 to CAV1 in HEK-293T cells. (D) The binding of Trx-1 to CAV1 in J774A.1 cells treated with Auranofin, GA or DNCB. (E) The interaction between Trx-1 and anti-Myc beads treated with the indicated concentrations of oxidants and antioxidants. The flow-through is the unbound fraction after oxidant or antioxidant treatment. (F) The binding of WT or C32/35S Trx-1 to CAV1 in HEK-293T cells treated with Auranofin. (G) Schematic representation of the CAV1 domain (top). The binding of full length or various mutants of CAV1 to Trx-1 in HEK-293T cells (bottom). The values are expressed as the mean ± SD, $^{**}p < 0.01$.

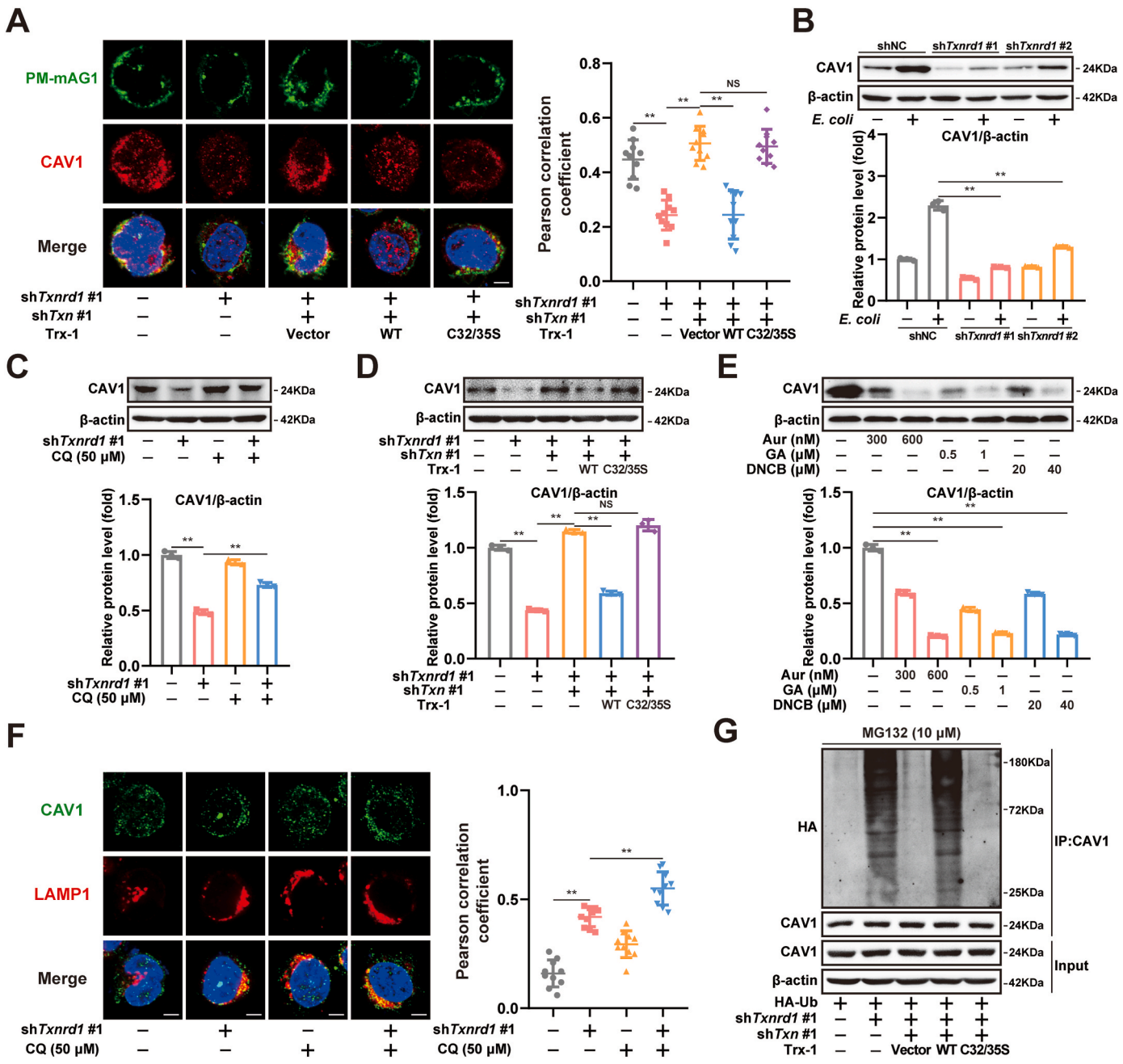

Fig. 7. TrxR1 maintains CAV1 cellular membrane localization and protein levels. (A) Intracellular distribution of CAV1 and PM-mAG1 in J774A.1 cells expressing Txnrd1 and Txn shRNA and Txn WT or C32/35S variant cDNA. Scale bars: 10 μm. Pearson's correlation coefficients for the co-localization of CAV1 with PM-mAG1 from multiple confocal images. n = 10 per group. (B) Western blot analysis of CAV1 expression in *E. coli*-infected J774A.1 cells upon Txnrd1 knockdown. n = 3 per group. (C) Western blot analysis of CAV1 expression in J774A.1 cells upon Txnrd1 knockdown treated with CQ. n = 3 per group. (D) Western blot analysis of CAV1 expression in J774A.1 cells expressing Txnrd1 and Txn shRNA and Txn WT or C32/35S variant cDNA. n = 3 per group. (E) Western blot analysis of CAV1 expression in J774A.1 cells treated with Auranofin, GA or DNCB. n = 3 per group. (F) Intracellular distribution of LAMP and CAV1 in J774A.1 cells upon Txnrd1 knockdown treated with CQ. Scale bars: 10 μm. Pearson's correlation coefficients for the co-localization of LAMP with CAV1 from multiple confocal images. n = 10 per group. (G) Analysis of ubiquitination of CAV1 in J774A.1 cells expressing Txnrd1 and Txn shRNA and Txn WT or C59S variant cDNA. The values are expressed as the mean ± SD, $^{**}p < 0.01$.

degradation. Correspondingly, our findings revealed a significant decrease in CAV1 protein expression levels upon Txnrd1 knockdown (Fig. 7B). Notably, CAV1 mRNA levels remained unchanged, suggesting that TrxR1 may play a role in promoting the degradation of CAV1 (Fig. S6A). CAV1, a membrane-anchored protein, is known to undergo lysosomal degradation (Hayeret al,2010). In line with these observations, our investigations demonstrate that inhibiting proteasomes has no discernible impact on the downregulation of CAV1 induced by Txnrd1 knockdown (Fig. S6B). However, lysosomal inhibition effectively rescues the diminished CAV1 levels resulting from Txnrd1 knockdown (Fig. 7C). Furthermore, simultaneous knockdown of Txnrd1 and Txn resulted in an increase in CAV1 expression. Upon the reintroduction of wild-type Trx-1, the downregulation of CAV1 induced by Txnrd1 knockdown was restored, while the reintroduction of the mutated Trx-1 failed to exhibit this restorative effect (Fig. 7D). Notably, direct treatment with oxidants or reductants had no impact on CAV1 expression (Fig. S6C); only the inhibition of TrxR1 significantly reduced CAV1 levels (Fig. 7E). Txnrd1 knockdown markedly facilitated the entry of

CAV1 into LAMP-positive lysosomes, with the lysosomal inhibitor CQ further exacerbating the intracellular accumulation of CAV1 (Fig. 7F). Additionally, the lysosomal degradation of CAV1 is dependent on ubiquitination modification. We assessed the polyubiquitination levels of CAV1 and found that Txnrd1 knockdown promotes the ubiquitination of CAV1. Simultaneous knockdown of Txnrd1 and Txn significantly inhibited the ubiquitination of CAV1. Upon the reintroduction of wild-type Trx-1, the promotion of CAV1 ubiquitination induced by Txnrd1 knockdown was restored, whereas the reintroduction of the mutated Trx-1 did not exhibit this restorative effect (Fig. 7G). These data indicate that TrxR1 plays a role in maintaining the cellular membrane localization and protein levels of CAV1.

2.9. TrxR1 modulates pyroptosis by downregulating of CAV1

To elucidate the role of CAV1 in TrxR1-mediated regulation of pyroptosis, we expressed CAV1 upon Txnrd1 knockdown (Fig. S7A). It is demonstrated that the expression of CAV1 upon Txnrd1 knockdown significantly reduces cell viability (Fig. 8A). Additionally, Txnrd1 knockdown markedly decreases LDH release, while the expression of CAV1 significantly increases LDH release (Fig. 8B). Similar changes are observed in the secretion of IL-1β (Fig. 8C). Importantly, the significant decrease in Caspase-11 (p26) activation, and GSDMD-N formation observed in Txnrd1-knockdown macrophages is reversed by the expression of CAV1 (Fig. 8D). Furthermore, the inhibitory effect of Txnrd1 knockdown on cytoplasmic LPS levels is also reversed by the expression of CAV1 (Fig. 8E). Observation of OMV internalization reveals that Txnrd1 knockdown significantly reduces cellular uptake of OMVs, while the expression of CAV1 significantly increases OMV internalization (Fig. 8F). Moreover, the inhibitory effect of Txnrd1 knockdown on CTxB internalization is reversed by the expression of CAV1 (Fig. S8B). These results collectively suggest that TrxR1-mediated pyroptosis is dependent on the downregulating of CAV1 (see Fig. 9).

3. Discussion

In this study, we found that Auranofin alleviates CLP-induced sepsis *in vivo* and inhibits the activation of Caspase-11 in vitro. As an inhibitor of TrxR, Auranofin exerts anti-inflammatory effects by promoting the formation of oxidized Trx-1 [26,27]. Although numerous studies have confirmed that Trx-1 interacts with other proteins during disulfide bond reduction, oxidized Trx-1 has been found to interact with NLRP1, mediating innate immune responses [25]. Our study confirms that oxidized Trx-1, through interaction with CAV1, leads to the lysosomal degradation of CAV1. During the infection process with Gram-negative bacteria, OMVs containing LPS are internalized into macrophages, mediating the activation of Caspase-11 [28,29]. Inhibiting TrxR1-induced formation of oxidized Trx-1 suppresses Caspase-11 activation and pyroptosis by blocking OMV internalization during Gram-negative bacterial infection. This sheds light on the anti-inflammatory potential of Auranofin through the modulation of the TrxR1-Trx-1 axis in the context of oxidative stress and innate immune responses.

Auranofin, an oral anti-rheumatic drug, exhibits potent anti-inflammatory activity, yet the mechanisms remain unclear [30,31]. Our results demonstrate that Auranofin alleviates *E. coli* infection-induced activation of Caspase-11 and pyroptosis. Auranofin has been identified as an inhibitor of TrxR, but TrxR exists in multiple subtypes, making it challenging to determine its molecular mechanism [32,33]. We individually constructed macrophages with knockdown Txnrd1 and Txnrd2, revealing that only Txnrd1 knockdown inhibits pyroptosis induced by *E. coli* infection, while Txnrd2 does not exert such an effect. TrxR1, as a widely distributed reductase, plays a crucial role in maintaining cellular redox balance [34–36]. Through the construction of a TrxR1 enzymatic site mutant, we confirmed that the regulatory role of TrxR1 in pyroptosis induced by *E. coli* infection depends on the enzymatic activity of TrxR1. Oxidized Trx-1 acts as a substrate for TrxR1 to regain reducing activity [37]. Consequently, by simultaneously knocking down Txnrd1 and Txn in macrophages, we found that the regulatory effect of TrxR1 on Caspase-11 activation and pyroptosis depends on the expression of Trx-1. TrxR1, as a reductase, contributes to maintaining the reducing activity of Trx-1 [38]. Therefore, by constructing a C32/35S mutant of Trx-1, we confirmed that the regulatory role of TrxR1 in pyroptosis is associated with the reducing activity site of Trx-1. Similar effects were observed with other TrxR1 inhibitors. These results substantiate the notion that the regulation of Trx-1 reducing activity by TrxR1 may be involved in Caspase-11 activation and pyroptosis.

The process of Gram-negative bacterial infection activating Caspase-11 involves intricate steps, including internalization of OMVs carrying LPS, early endosomal trafficking of LPS, and cytoplasmic release [16,17,29]. Initially, we observed that inhibiting TrxR1 reduced the aggregation of LPS in early endosomes. Early endosomes undergo sorting to mature and subsequently fuse with lysosomes for degradation [39]. Therefore, the inhibition of LPS aggregation in early endosomes might be related to endosomal maturation or lysosomal degradation. However, inhibiting TrxR1 also reduced the co-localization of LPS with late endosomes. Interestingly, inhibiting lysosomal degradation did not reverse the decrease in cytoplasmic LPS. These results suggest that TrxR1 does not affect the trafficking and maturation of LPS in endosomes, indicating a potential impact on OMV internalization. By fluorescently labeling OMVs, we confirmed that Txnrd1 knockdown inhibits OMV internalization. OMV internalization involves clathrin-mediated endocytosis and caveolin-mediated endocytosis. CTxB uptake experiments confirmed that Txnrd1 knockdown might impede caveolin-mediated endocytosis. By adding two caveolin-mediated endocytosis inhibitors, we confirmed that inhibiting caveolin-mediated endocytosis disrupts Caspase-11 activation. These results indicate that TrxR1, through regulating the internalization of OMVs, influences the cytoplasmic levels of LPS.

Despite confirming that TrxR1 regulates Caspase-11 activation and pyroptosis depending on the reductive activity of Trx-1, inhibiting TrxR1 results in the presence of oxidized Trx-1. We observed that the interaction between Trx-1 and CAV1 relies on the active site cysteines of Trx-1. Importantly, this interaction occurs exclusively with the oxidized form of Trx-1. Furthermore, this interaction influences the cellular membrane localization of CAV1. Additionally, we found that inhibiting TrxR1 promotes lysosomal-dependent degradation of CAV1. The lysosomal degradation of CAV1 is solely associated with the oxidative-reductive state of Trx-1, independent of cellular oxidative stress. Moreover, by overexpressing CAV1 upon Txnrd1 knockdown, we confirmed that the inhibitory effect of Txnrd1 knockdown on Caspase-11 and pyroptosis is partially reversed. These results indicate that TrxR1, by modulating the oxidative-reductive status of Trx-1, regulates the endocytic activity mediated by CAV1.

In summary, our results suggest that Auranofin attenuates sepsis-induced inflammation and tissue damage in mice. Mechanistic studies confirm that the inhibitory effect of Auranofin on the Caspase-11 inflammasome depends on TrxR1's regulation of the oxidative-reductive status of Trx-1. Furthermore, our research reveals that inhibiting TrxR1 leads to the stabilization of oxidized Trx-1, thereby binding to CAV1 and hindering its membrane localization, promoting lysosomal degradation. Therefore, inhibiting TrxR1 holds promise as a viable therapeutic strategy for the treatment of lethal infections. Nevertheless, further exploration is needed to elucidate the precise mechanisms involved.

4. Materials and methods

4.1. Reagents and antibodies

Auranofin (Aur, Cat No. HY-B1123), Gambogic Acid (GA, Cat No.

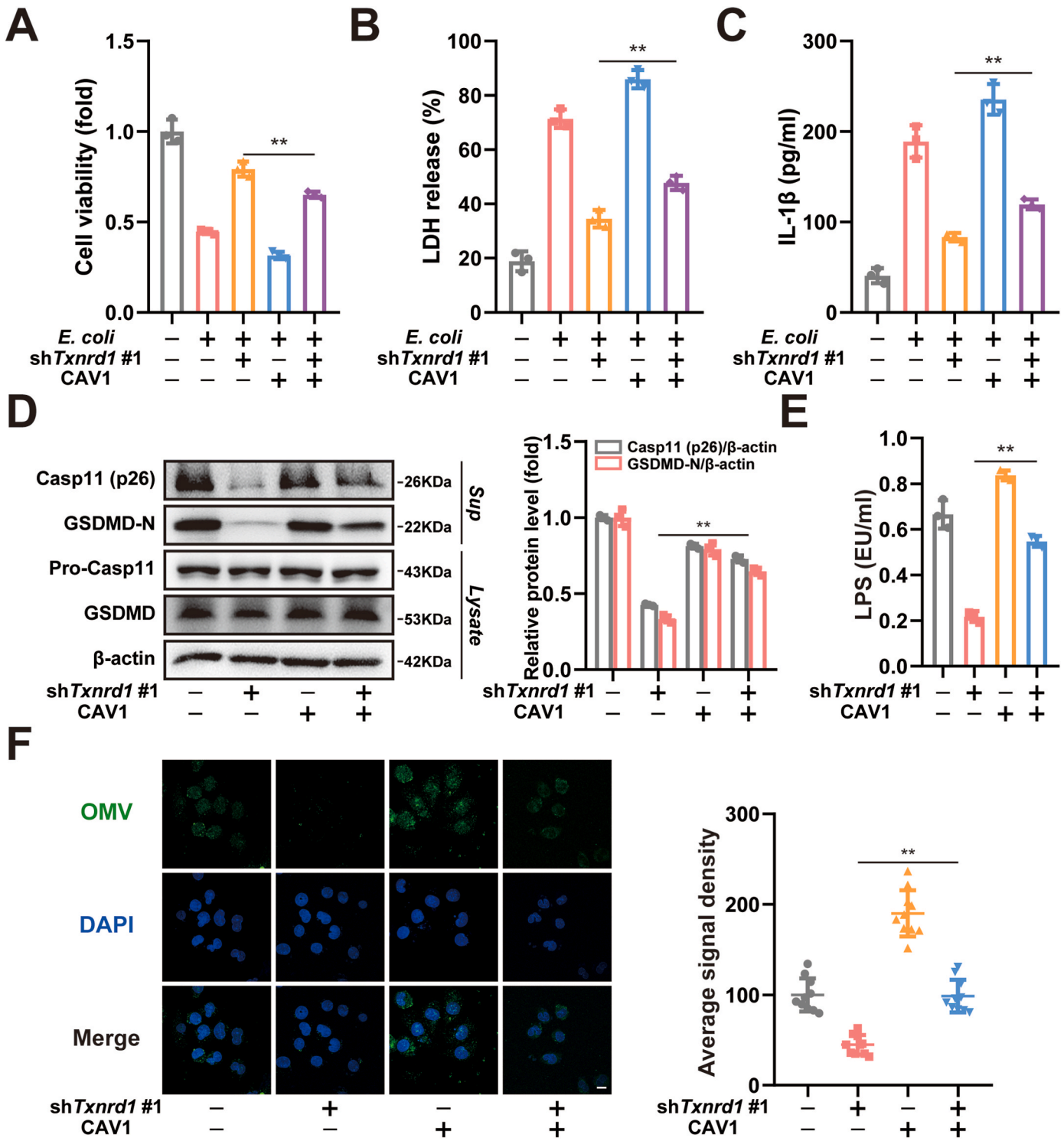

Fig. 8. Overexpression of CAV1 rescued TrxR1-regulated pyroptosis and Caspase-11 inflammasome activation. (A) Analysis of cell viability in *E. coli*-infected J774A.1 cells expressing Txnrd1 shRNA and CAV1 cDNA. n = 3 per group. (B) Analysis of LDH release in *E. coli*-infected J774A.1 cells expressing Txnrd1 shRNA and CAV1 cDNA. n = 3 per group. (C) Analysis of IL-1β in supernatants of *E. coli*-infected J774A.1 cells expressing Txnrd1 shRNA and CAV1 cDNA. n = 3 per group. (D) Western blot analysis of Caspase-11 and GSDMD expression in supernatants (Sup) and lysate in *E. coli*-infected J774A.1 cells expressing Txnrd1 shRNA and CAV1 cDNA. n = 3 per group. (E) LAL assay for LPS (EU, endotoxin units) in the cytosolic fractions of *E. coli*-infected J774A.1 cells expressing Txnrd1 shRNA and CAV1 cDNA. n = 3 per group. (F) The endocytosis of DiO-labeled OMVs in J774A.1 cells expressing Txnrd1 shRNA and CAV1 cDNA. Scale bars: 10 μm. The average signal density of internalized green fluorescent OMVs. n = 10 per group.The values are expressed as the mean ± SD, $^{**}p < 0.01$. (For interpretation of the references to colour in this figure legend, the reader is referred to the Web version of this article.)

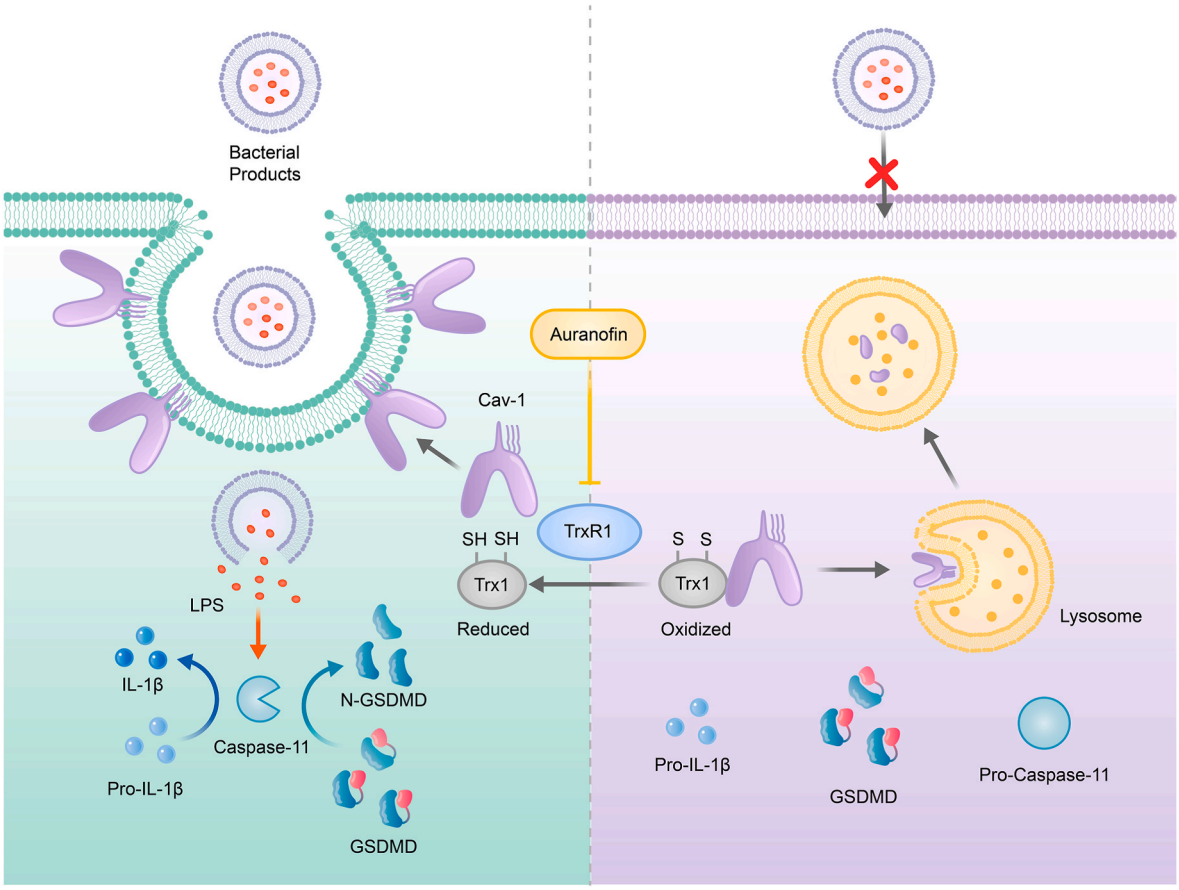

Fig. 9. Role of TrxR1 inhibition by Auranofin in preventing Caspase-11 induced pyroptosis. TrxR1 plays a crucial role in controlling the redox state of Trx-1, thereby affecting pyroptosis. By inhibiting TrxR1, Auranofin keeps Trx-1 in an oxidized state, which influences Caveolin-1 mediated OMV internalization and prevents pyroptosis triggered by Caspase-11 activation.

HY-N0087) Chloroquine (CQ, Cat No. HY-17589A) were purchased from MCE (Med Chem Express). DNCB (Cat No. 237329) and H_2O_2 (Cat No.88597) were purchased from Sigma–Aldrich (St. Louis, USA). Aur, GA and CQ were dissolved in dimethyl sulfoxide (DMSO), the storing concentrations of the reagents used are 1 mM, 1 mM and 10 mM. For *in vivo* experiments, Aur was dissolved at 10 % DMSO and 90 % Corn Oil for intraperitoneal injection.

Triton X-100 was purchased from Shanghai Chao Rui Biotech. Co. Ltd. (Shanghai, China). ELISA kits for mouse IL-1β (RK00006), TNF-*α* (RK00027) and IL-18 (RK00104) were purchased from ABclonal Biotechnology Co. Ltd. (Wuhan, China).

Primary antibodies against Caspase-11 (A0964), GSDMD (A24476), IL-1β (A16288), EEA1 (A0592), Rab7 (A12308), LAMP (A1961), TrxR1 (A4725), TrxR2 (A8884), Trx-1 (A4024), CAV1 (A19006), Na^+/K^+-ATPase (A12405), DDDDK-Tag (AE005), Myc-Tag (AE010), HA-Tag (AE008) and β-actin (AC006) were from ABclonal Biotechnology Co. Ltd. Antibodies against CAV1 (66067-1-Ig) was from Proteintech. HRP goat anti-mouse IgG (H + L; AS003) and HRP goat anti-rabbit IgG (H + L; AS014) were from ABclonal. High-sig ECL Western Blotting Substrate was from Tanon (180–5001). Alexa Fluor 488 donkey anti-rabbit IgG (A11008) and Alexa Fluor 594 donkey anti-mouse IgG (A31570) were obtained from Invitrogen. Dye DAPI was purchased from Invitrogen (Carlsbad, USA). Alexa555-conjugated Cholera Toxin Subunit B (CTxB, C34776) was purchased from Thermo Fisher. Annexin V-FITC/PI Apoptosis Detection Kit (Cat No.KGA1102) was purchased from Keygen Biotechnology (Nanjing, China). LDH Release Assay Kit (Cat No.C0016) was purchased from Beyotime Biotechnology (Shanghai, China). Cell Counting Kit (CCK-8, Cat No.40203ES60) was purchased from Yeasen Biotechnology (Shanghai, China). Chromogenic Endotoxin Quant Kit (Cat No.A39552S) was purchased from Thermo Fisher.

4.2. Mice

Six-to eight-week-old male C57BL/6J mice weighing 18–22 g were procured from the Shanghai Laboratory Animal Center, China Academy of Sciences. During the study, the animals were provided with ad libitum access to food and water and were kept in a 12 h light/dark cycle at a controlled temperature of 21 ± 2 °C with a relative humidity of 45 ± 10 %. Laboratory animals were randomly assigned to groups of equal size. All animal samples were analyzed in a blinded manner. All animal care and experimental procedures were conducted in accordance with the guidelines approved by the University Committee on Use and Care of Animals at the China Pharmaceutical University. The animal studies are reported in accordance with the ARRIVE guidelines.

4.3. Animal model of sepsis

Sepsis was induced in C57BL/6J mice through cecal ligation and puncture. The mice were divided into control, model and Aur treatment groups. Prior to surgery, mice in the model and Aur treatment groups fasted for 16 h with access to water. Anesthesia was administered, and a careful abdominal incision exposed the cecum without damaging blood vessels. The cecum was ligated and punctured before being returned to the abdomen. The incision was sutured, and saline was given to compensate for fluid loss. In the control group, the same anesthesia was applied without cecum manipulation. Post-surgery, mice had unrestricted access to food and water. In the model group, mice received intraperitoneal injections of 10 % DMSO and 90 % Corn Oil before and

after cecal ligation. In the Aur treatment group, mice were injected with Aur (5 mg/kg) at specified intervals before and after cecal ligation.

4.4. Detection of bacterial burden

On the fourth day following the establishment of the CLP model, blood was collected from mice on a sterile bench. Mouse blood was collected in a sterile anticoagulant tube, while 5 ml of sterilized LB liquid medium was placed in a sterilized centrifuge tube. Subsequently, 10 μl of blood was added to the LB medium and incubated overnight on a shaker at 37 °C. The next day, the absorbance was measured at a wavelength of 600 nm.

4.5. Detection of LDH, BUN and ALT

On the fourth day following the establishment of the CLP model, blood was collected from mice on a sterile bench. After a 30 min static incubation, the tube was centrifuged at 4 °C and 3000 rpm for 10 min. The upper serum layer was then transferred into a new 1.5 ml EP tube. Reagent parameters were set based on the instructions, and LDH, BUN, and ALT levels were measured using a blood biochemistry analyzer.

4.6. Hematoxylin and Eosin staining

Paraffin-embedded colon sections were respectively deparaffinized and stained with Hematoxylin and Eosin.

4.7. Cell culture

The murine macrophage J774A.1 cell line was purchased from the American Type Culture Collection (ATCC). The cells were cultured with DMEM medium (Gibco, Carlsbad, USA) supplemented with 10 % (*v/v*) fetal bovine serum (Gibco, Carlsbad, USA), 100 U/ml benzylpenicillin and 100 mg/m streptomycin. Bone marrow-derived macrophages (BMDM) were isolated from C57BL/6 mice and cultured with DMEM medium (Gibco, Carlsbad, USA) supplemented with 10 % (*v/v*) fetal bovine serum (Gibco, Carlsbad, USA) and 20 ng/ml GM-CSF (Pepro-Tech, NJ, USA). Cells were harvested and seeded on cell culture dishes (60 mm × 15 mm). Exchanging culture medium every 3 d, adherent macrophages were obtained within about one week. Cells were cultured in a humidified environment with 5 % CO_2 at 37 °C.

4.8. Cell viability assay

The CCK-8 reagent (Beyotime, Shanghai, China) was used for detection according to the user's manual. In brief, J774A.1 or BMDMs cells in the logarithmic growth phase were cultured at a density of 2 × 10^4 cells/ml in a 96-well plate. Following specified treatments, cells were washed with PBS, and 10 μl of a 10 % diluted CCK-8 solution was added to each well. The plates were then incubated for approximately 90 min at 37 °C in a CO_2 incubator. Absorbance at 450 nm was measured using a microplate reader (Molecular Devices, Sunnyvale, CA, USA). Cell viability was calculated as a percentage using the mean optical density (OD) values from three replicate wells per treatment group, according to the formula: Cell viability (%)=($OD_{treatment\ group}/OD_{control\ group}$) × 100 %.

4.9. PI uptake assay

After the J774A.1 and BMDMs were seeded in 6-well plates, the medium was replaced once the cell density reached approximately 60 %. Following the infection with *E. coli*, macrophages underwent apoptosis, and the culture medium was then discarded. The cells were washed twice with PBS and treated with 200 μl of binding buffer, containing 2.5 μl of PI, followed by incubation at room temperature for 15–20 min. The cells were washed 3 times with PBS and then observed for cell morphology and image acquisition using bright-field and fluorescence microscopy. Throughout the entire experimental procedure, precautionary measures were implemented to prevent light exposure.

4.10. Cytokine quantification by enzyme-linked immunoassay

IL-1β, TNF-*α* and IL-18 production in the mice serum were measured by ELISA kits according to the manufacturers' recommendations.

4.11. Cellular TrxR activity

J774A.1 cells were plated in 6-well plates and treated with various concentrations of Auranofin. After treatment, cells were collected and washed twice with ice-cold PBS. Total cellular proteins were extracted using RIPA buffer on ice for 30 min. TrxR activities in the cell lysates were measured using the endpoint Trx-1-coupled insulin assay [40]. In brief, an appropriate volume of cell lysate was added to a master mixture containing 80 mM Hepes buffer (pH 7.5), 15 μM Trx-1, 300 μM insulin, 660 μM NADPH, and 3 mM EDTA. A reaction mixture without Trx-1 served as a background control. Samples were incubated at 37 °C for 30 min. Subsequently, 6.0 M guanidine hydrochloride (GuHCl) containing 1 mM DTNB and 20 mM EDTA (pH 7.5) was added to each well, and the entire microplate was shaken for 10 s. The endpoint absorbance at 412 nm was then measured for each well, using wells without enzymes as blanks. The TrxR activities in the cell lysates were normalized to protein concentration to ensure accurate comparisons.

4.12. Fluorescent labeling of OMVs

Outer membrane vesicles (2 mg/ml) were labeled with 1 % (*v/v*) 3,3′-dioctadecyloxacarbocyanine perchlorate (DiO; Molecular Probes, USA) for 20 min at 37 °C [41]. Excess dye was removed by washing OMVs three times with PBS using a 10 kDa MW CO filtration column (Amicon).

4.13. Immunofluorescence

Fixed cells were prepared for confocal imaging by fixing them with 4 % paraformaldehyde in PBS, permeabilizing them with 0.5 % Triton X-100, and blocking them with 3 % BSA for 1 h. The samples were incubated overnight at 4 °C with primary antibodies diluted 1:100. The samples were incubated overnight at 4 °C with primary antibodies diluted 1:100. Subsequently, the cells were washed three times with PBS and stained with DAPI. Finally, the slides were imaged using a confocal laser scanning microscopeta (Fluoview^{TM} FV3000, Olympus, Japan). Data analysis was conducted using ImageJ software, focusing on quantifying fluorescence intensity and calculating the pearson correlation coefficient for colocalization studies.

4.14. RNA isolation and qPCR

RNA was isolated from cells and reverse transcribed, and qPCR was performed as previously described [42]. Primer sequences are as follows:

Mouse *Cav1*-sense (5′- CCGTGCATCAAGAGCTTCCT-3′);
Mouse *Cav1*-antisense (5′- CTCTTTCTGCGTGCTGATGC-3′);
Mouse *18s*-sense (5′-CGATCCCAGGGCCTCACTA -3′);
Mouse *18s* -antisense (5′-AGTCCCTGCCCTTTGTACACA -3′).

4.15. Western blot analysis

Proteins were extracted by incubating the cell pellet or tissue in RIPA buffer containing 1 % PMSF and 1 % phosphatase inhibitors. Protein concentration was quantified using a BCA protein quantification kit. The proteins were separated using sodium dodecyl sulfate-polyacrylamide gel electrophoresis (SDS-PAGE) and subsequently transferred to a nitrocellulose membrane. Following a 1 h blocking step at room

temperature with 5 % BSA, the membrane was then incubated with primary antibodies overnight at 4 °C. The membrane was washed with PBST, incubated with horseradish peroxidase (HRP)-labeled secondary antibodies at room temperature for 1 h. Detection was performed using an enhanced chemiluminescence (ECL) reagent and visualized on a Tanon 5200 automatic luminescence imaging system. Protein levels were normalized to β-actin and quantified using ImageJ software.

4.16. Co-immunoprecipitation (Co-IP) analysis

After processing as required, approximately 200 μl volum cells were collected in 1.5 ml EP tube. Cells were lysed by adding 1 ml of Co-IP lysis buffer (50 mM HEPES, 150 mM NaCl, 1 mM EDTA, 0.5 % NP-40, 1 mM PMSF, and 1x protease inhibitor cocktail) and incubating on ice for 10 min. Subsequently, the lysate was centrifuged at 14000 g for 10 min at 4 °C. Concurrently, 50 μl of protein A/G magnetic beads (MCE, NJ, USA) were incubated with the specified antibodies for each experiment at room temperature for 30 min. Using a magnetic rack or centrifugation, separate the magnetic beads and discard the supernatant. Wash the beads with 400 μl of lysis buffer on ice, and agitate on a shaker for 5 min. Repeat this washing process 4 times. After washed 4 times, the beads were added in each sample and rotated over night at 4 °C. The next day, the beads were washed 4 times and boiled with loading buffer. Then the bounded protein was detected by SDS-PAGE.

4.17. Statistical analysis

The data shown in the study were obtained in at least three independent experiments and all results represent the mean ± SD. Differences between the groups were assessed by one-way ANOVA test. Details of each statistical analysis used are provided in the figure legends. Differences with P values < 0.05 were considered statistically significant.

CRediT authorship contribution statement

Dongsheng Bai: Data curation. **Chen Zhou:** Formal analysis. **Jiaying Du:** Investigation. **Jiawei Zhao:** Methodology. **Chunyang Gu:** Software. **YuXiang Wang:** Validation. **Lulu Zhang:** Visualization. **Na Lu:** Writing – review & editing. **Yue Zhao:** Writing – original draft, Conceptualization.

Declaration of competing interest

All authors declare that they have no conflict of interest.

Data availability

Data will be made available on request.

Acknowledgments

This work was supported by the National Natural Science Foundation of China (No. 82373910, 82204409). The “Double First-Class” University (CPU2022QZ20). We thank Mrs. Liuyi Zhong from Pharmaceutical Animal Experimental Center in China Pharmaceutical University for her kind help in the *in vivo* experiments.

Appendix A. Supplementary data

Supplementary data to this article can be found online at https://doi.org/10.1016/j.redox.2024.103277.

References

[1] S.M. Opal, Endotoxins and other sepsis triggers, Contrib. Nephrol. 167 (2010) 14–24.
[2] D. Rallis, M. Lithoxopoulou, S. Pervana, P. Karagianni, I. Hatziioannidis, V. Soubasi, et al., Clinical chorioamnionitis and histologic placental inflammation: association with early-neonatal sepsis, J. Matern. Fetal Neonatal Med. 35 (25) (2022) 8090–8096.
[3] C.L. Lakshmikanth, S.P. Jacob, V.H. Chaithra, H.C. de Castro-Faria-Neto, G. K. Marathe, Sepsis: in search of cure, Inflamm. Res. 65 (8) (2016) 587–602.
[4] R. Yang, X. Zhang, A potential new pathway for heparin treatment of sepsis-induced lung injury: inhibition of pulmonary endothelial cell pyroptosis by blocking hMGB1-LPS-induced caspase-11 activation, Front. Cell. Infect. Microbiol. 12 (2022) 984835.
[5] L. Kiczak, U. Paslawska, W. Gozdzik, B. Adamik, M. Zielinska, S. Zielinski, et al., Effect of low-dose hydrocortisone and inhaled nitric oxide on inflammatory mediators and local pulmonary metalloproteinases activity in LPS-induced sepsis in piglets, Sci. Rep. 13 (1) (2023) 11369.
[6] B. Zhai, L.S. Ma, R.Q. Shen, J. Yu, Y.N. Tao, A.P. Xu, et al., [Caspase-1/-11 participates in LPS-induced sepsis-associated acute kidney injury by cleaving GSDMD], Sheng Li Xue Bao 75 (1) (2023) 10–16.
[7] B.E. Burdette, A.N. Esparza, H. Zhu, S. Wang, Gasdermin D in pyroptosis, Acta Pharm. Sin. B 11 (9) (2021) 2768–2782.
[8] Ct Drummer, F. Saaoud, N.C. Jhala, R. Cueto, Y. Sun, K. Xu, et al., Caspase-11 promotes high-fat diet-induced NAFLD by increasing glycolysis, OXPHOS, and pyroptosis in macrophages, Front. Immunol. 14 (2023) 1113883.
[9] W. Xu, X. Huang, W. Li, G. Qian, B. Zhou, X. Wang, et al., Carbon monoxide ameliorates lipopolysaccharide-induced acute lung injury via inhibition of alveolar macrophage pyroptosis, Exp. Anim. 72 (1) (2023) 77–87.
[10] C. Ye, W. Li, Y. Yang, Q. Liu, S. Li, P. Zheng, et al., Inappropriate use of antibiotics exacerbates inflammation through OMV-induced pyroptosis in MDR Klebsiella pneumoniae infection, Cell Rep. 36 (12) (2021) 109750.
[11] C. Yuan, K. Ai, M. Xiang, C. Xie, M. Zhao, M. Wu, et al., Novel 1-hydroxy phenothiazinium-based derivative protects against bacterial sepsis by inhibiting AAK1-mediated LPS internalization and caspase-11 signaling, Cell Death Dis. 13 (8) (2022) 722.
[12] D. Augustyniak, T. Olszak, Z. Drulis-Kawa, Outer membrane vesicles (OMVs) of Pseudomonas aeruginosa provide passive resistance but not sensitization to LPS-specific phages, Viruses 14 (1) (2022).
[13] A. Pfalzgraff, W. Correa, L. Heinbockel, A.B. Schromm, C. Lubow, N. Gisch, et al., LPS-neutralizing peptides reduce outer membrane vesicle-induced inflammatory responses, Biochim. Biophys. Acta Mol. Cell Biol. Lipids 1864 (10) (2019) 1503–1513.
[14] E.Y. Shin, N.K. Soung, M.A. Schwartz, E.G. Kim, Altered endocytosis in cellular senescence, Ageing Res. Rev. 68 (2021) 101332.
[15] H. Parker, K. Chitcholtan, M.B. Hampton, J.I. Keenan, Uptake of Helicobacter pylori outer membrane vesicles by gastric epithelial cells, Infect. Immun. 78 (12) (2010) 5054–5061.
[16] A. Sivanantham, W. Alktaish, S. Murugeasan, B. Gong, H. Lee, Y. Jin, Caveolin-1 regulates OMV-induced macrophage pro-inflammatory activation and multiple Toll-like receptors, Front. Immunol. 14 (2023) 1044834.
[17] H.B. Thapa, P. Kohl, F.G. Zingl, D. Fleischhacker, H. Wolinski, T.A. Kufer, et al., Characterization of the inflammatory response evoked by bacterial membrane vesicles in intestinal cells reveals an RIPK2-dependent activation by enterotoxigenic Escherichia coli vesicles, Microbiol. Spectr. 11 (4) (2023) e0111523.
[18] B.C. Liu, J. Sarhan, A. Panda, H.I. Muendlein, V. Ilyukha, J. Coers, et al., Constitutive interferon maintains GBP expression required for release of bacterial components upstream of pyroptosis and anti-DNA responses, Cell Rep. 24 (1) (2018) 155–168 e155.
[19] P. Bao, Y. Gong, Y. Wang, M. Xu, Z. Qian, X. Ni, et al., Hydrogen sulfide prevents LPS-induced depression-like behavior through the suppression of NLRP3 inflammasome and pyroptosis and the improvement of mitochondrial function in the Hippocampus of mice, Biology 12 (8) (2023).
[20] P. Zhang, M. Zang, Z. Sang, Y. Wei, Y. Yan, X. Bian, et al., Vitamin C alleviates LPS-induced myocardial injury by inhibiting pyroptosis via the ROS-AKT/mTOR signalling pathway, BMC Cardiovasc. Disord. 22 (1) (2022) 561.
[21] Y. Liu, W. Min, Thioredoxin promotes ASK1 ubiquitination and degradation to inhibit ASK1-mediated apoptosis in a redox activity-independent manner, Circ. Res. 90 (12) (2002) 1259–1266.
[22] S.I. Hashemy, A. Holmgren, Regulation of the catalytic activity and structure of human thioredoxin 1 via oxidation and S-nitrosylation of cysteine residues, J. Biol. Chem. 283 (32) (2008) 21890–21898.
[23] H. Li, A. Wan, G. Xu, D. Ye, Small changes huge impact: the role of thioredoxin 1 in the regulation of apoptosis by S-nitrosylation, Acta Biochim. Biophys. Sin. 45 (3) (2013) 153–161.
[24] Z. Xu, H. Hu, K. Wang, Z. Zhou, X. He, X. Huang, et al., Sinensetin, a polymethoxyflavone from citrus fruits, ameliorates LPS-induced acute lung injury by suppressing Txnip/NLRP3/Caspase-1/GSDMD signaling-mediated inflammatory responses and pyroptosis, Food Funct. (2024).
[25] J. Jia, X. Zhang, G. Xu, X. Zeng, L. Li, Thioredoxin-1 inhibits amyloid-beta(25-35)-induced activation of NLRP1/caspase-1/GSDMD pyroptotic pathway in PC12 cells, Mol. Biol. Rep. 49 (5) (2022) 3445–3452.
[26] H. Hwangbo, S.Y. Ji, M.Y. Kim, S.Y. Kim, H. Lee, G.Y. Kim, et al., Anti-inflammatory effect of auranofin on palmitic acid and LPS-induced inflammatory response by modulating TLR4 and NOX4-mediated NF-kappaB signaling pathway in RAW264.7 macrophages, Int. J. Mol. Sci. 22 (11) (2021).
[27] H.A. Rothan, S. Stone, J. Natekar, P. Kumari, K. Arora, M. Kumar, The FDA-approved gold drug auranofin inhibits novel coronavirus (SARS-COV-2) replication and attenuates inflammation in human cells, Virology 547 (2020) 7–11.

[28] P. Deo, S.H. Chow, M.L. Han, M. Speir, C. Huang, R.B. Schittenhelm, et al., Mitochondrial dysfunction caused by outer membrane vesicles from Gram-negative bacteria activates intrinsic apoptosis and inflammation, Nat. Microbiol. 5 (11) (2020) 1418–1427.
[29] N.P. Giordano, M.B. Cian, Z.D. Dalebroux, Outer membrane lipid secretion and the innate immune response to gram-negative bacteria, Infect. Immun. 88 (7) (2020).
[30] M. Yamashita, Auranofin: past to present, and repurposing, Int. Immunopharm. 101 (Pt B) (2021) 108272.
[31] H. Hwangbo, M.Y. Kim, S.Y. Ji, S.Y. Kim, H. Lee, G.Y. Kim, et al., Auranofin attenuates non-alcoholic fatty liver disease by suppressing lipid accumulation and NLRP3 inflammasome-mediated hepatic inflammation in vivo and in vitro, Antioxidants 9 (11) (2020).
[32] R. Yang, S. Sun, Y. Guo, Y. Meng, H. Liu, M. Shi, et al., Anti-inflammatory effect of dimethyl fumarate associates with the inhibition of thioredoxin reductase 1 in RAW 264.7 cells, Molecules 28 (1) (2022).
[33] P. Sabatier, C.M. Beusch, R. Gencheva, Q. Cheng, R. Zubarev, E.S.J. Arner, Comprehensive chemical proteomics analyses reveal that the new TRi-1 and TRi-2 compounds are more specific thioredoxin reductase 1 inhibitors than auranofin, Redox Biol. 48 (2021) 102184.
[34] M. Caillot, F. Zylbersztejn, E. Maitre, J. Bourgeais, O. Herault, B. Sola, ROS overproduction sensitises myeloma cells to bortezomib-induced apoptosis and alleviates tumour microenvironment-mediated cell resistance, Cells 9 (11) (2020).
[35] S. Alshehri, S.F. Ahmad, N.A. Albekairi, S.S. Alqarni, N.O. Al-Harbi, L.Y. Al-Ayadhi, et al., Thioredoxin 1 and thioredoxin reductase 1 redox system is dysregulated in neutrophils of subjects with autism: in vitro effects of environmental toxicant, methylmercury, Toxics 11 (9) (2023).
[36] C.T. Shearn, A.L. Anderson, C.G. Miller, R.C. Noyd, M.W. Devereaux, N. Balasubramaniyan, et al., Thioredoxin reductase 1 regulates hepatic inflammation and macrophage activation during acute cholestatic liver injury, Hepatol. Commun. 7 (1) (2023) e0020.
[37] H. Lv, C. Zhu, W. Wei, X. Lv, Q. Yu, X. Deng, et al., Enhanced Keap1-Nrf2/Trx-1 axis by daphnetin protects against oxidative stress-driven hepatotoxicity via inhibiting ASK1/JNK and Txnip/NLRP3 inflammasome activation, Phytomedicine 71 (2020) 153241.
[38] J.W. Huang, Q.Y. Xu, M. Lin, B. Cheng, C. Ji, The extract from acidosasa longiligula alleviates in vitro UV-induced skin cell damage via positive regulation of thioredoxin 1, Clin. Interv. Aging 15 (2020) 897–905.
[39] M.C.Q. Houser, S.P.C. Mitchell, P. Sinha, B. Lundin, O. Berezovska, M. Maesako, Endosome and lysosome membrane properties functionally link to gamma-secretase in live/intact cells, Sensors 23 (5) (2023).
[40] E.S. Arner, A. Holmgren, Measurement of thioredoxin and thioredoxin reductase, Curr. Protoc. Toxicol. (2001) (Chapter 7): Unit 7 4.
[41] A.T. Irving, H. Mimuro, T.A. Kufer, C. Lo, R. Wheeler, L.J. Turner, et al., The immune receptor NOD1 and kinase RIP2 interact with bacterial peptidoglycan on early endosomes to promote autophagy and inflammatory signaling, Cell Host Microbe 15 (5) (2014) 623–635.
[42] Y. Zhao, Q. Guo, K. Zhao, Y. Zhou, W. Li, C. Pan, et al., Small molecule GL-V9 protects against colitis-associated colorectal cancer by limiting NLRP3 inflammasome through autophagy, OncoImmunology 7 (1) (2017) e1375640.